ADVANCED MATERIALS
www.advmat.de

Phonon Polaritonics in Broad Terahertz Frequency Range with Quantum Paraelectric $SrTiO_3$

*Rui Xu, Tong Lin, Jiaming Luo, Xiaotong Chen, Elizabeth R. Blackert, Alyssa R. Moon, Khalil M. JeBailey, and Hanyu Zhu**

Photonics in the frequency range of 5–15 terahertz (THz) potentially open a new realm of quantum materials manipulation and biosensing. This range, sometimes called "the new terahertz gap", is traditionally difficult to access due to prevalent phonon absorption bands in solids. Low-loss phonon–polariton materials may realize sub-wavelength, on-chip photonic devices, but typically operate in mid-infrared frequencies with narrow bandwidths and are difficult to manufacture on a large scale. Here, for the first time, quantum paraelectric $SrTiO_3$ enables broadband surface phonon–polaritonic devices in 7–13 THz. As a proof of concept, polarization-independent field concentrators are designed and fabricated to locally enhance intense, multicycle THz pulses by a factor of 6 and increase the spectral intensity by over 90 times. The time-resolved electric field inside the concentrators is experimentally measured by THz-field-induced second harmonic generation. Illuminated by a table-top light source, the average field reaches 0.5 GV m^{-1} over a large volume resolvable by far-field optics. These results potentially enable scalable THz photonics with high breakdown fields made of various commercially available phonon–polariton crystals for studying driven phases in quantum materials and nonlinear molecular spectroscopy.

1. Introduction

Recent development of terahertz (THz) spectroscopy and imaging have led to new fundamental scientific discoveries and applications in materials physics and biochemistry.[1,2] For example, THz coherent control of quantum materials becomes a promising means to elucidate the interaction mechanisms among electrons, lattice, and spins, as well as to create on-demand properties like superconductivity, ferroelectricity, topology, and magnetism.[3–9] Vibrational resonance-enhanced THz polarimetry and imaging, can reveal the long-range order of biomaterials, including chirality, intramolecular coupling, and interaction with water, as well as detect and manipulate cell membrane dynamics.[10–15] Many of these applications require a high electric field, widely tunable frequency range and polarization, and proper spatial resolution, which are more commonly available toward the high-frequency end (≳15 THz, ≲20 μm, or ≳62 meV) and low-frequency end (≲5 THz, ≳60 μm, or ≲21 meV), but less accessible for the range of 5–15 THz (20–60 μm) in between, which is sometimes called "the new terahertz gap".[1,2] This intermediate frequency range is important for resonant phonon-driven phenomena in quantum materials such as enhanced superconductivity in K_3C_{60} and magnetization in CeF_3,[16,17] as well as the characterization of nucleobases in biological studies.[18] Despite the tremendous progress, a free-space electric field up to GV m^{-1} in this frequency range can only be achieved with table-top sources under extreme conditions.[19–21] Many photonic structures can locally enhance field,[22–24] but there are few materials with low loss and high damage threshold for constructing devices in 5–15 THz.

Phonon polariton (PhP) materials, which are polar crystals that exhibit strong coupling between infrared photons and collective lattice vibrations (phonons), are promising for extending high-field, sub-wavelength photonics to the infrared and terahertz bands.[25–28] PhP materials exhibit much higher dielectric strengths and lower loss than plasmon polariton materials in applicable spectra ranges,[29,30] and have been employed to construct many photonic devices including infrared superlens, nano-antenna, biosensors, memory, and thermal radiators.[31–35] In particular, surface phonon polaritons (SPhP), confined at the interface between the phonon polaritonic and dielectric materials as thin as a monolayer, can be launched, guided, and focused in sub-wavelength and tunable structures.[36–41] However, most previous SPhP studies only focused on materials supporting SPhP

R. Xu, T. Lin, J. Luo, X. Chen, E. R. Blackert, K. M. JeBailey, H. Zhu
Department of Materials Science and NanoEngineering
Rice University
Houston, TX 77005, USA
E-mail: hanyu.zhu@rice.edu
J. Luo
Applied Physics Graduate Program
Rice University
Houston, TX 77005, USA
A. R. Moon
Nanotechnology Research Experience for Undergraduates (Nano REU) Program
Rice University
Houston, TX 77005, USA
The ORCID identification number(s) for the author(s) of this article can be found under https://doi.org/10.1002/adma.202302974

DOI: 10.1002/adma.202302974

at wavelengths below 15 µm.[26,42–49] Some III-V semiconductors show promise for expanding infrared photonics like emitters, waveguides, and resonators toward longer wavelengths but with very limited bandwidth due to the narrow PhP resonance of the materials.[50–54] Therefore, broadband SPhP materials for photonics in the new terahertz gap are urgently needed.

Here, we report phonon polaritonics in the new THz gap utilizing the quantum paraelectric $SrTiO_3$. Certain perovskite oxides are known to have ultrastrong light-phonon coupling, which leads to an ultrabroad coupling gap (called the Reststrahlen band).[55] In $SrTiO_3$, such strong coupling was attributed to the soft mode of ferroelectric instability.[56] Due to quantum fluctuations, this mode is not condensed or overdamped even at zero temperature, giving the name "quantum paraelectric". The relatively low-loss and low-frequency mode not only results in unique physics such as mesoscopic fluctuating domains and unusual superconductivity but also was theoretically suggested to enable THz phonon polaritonics.[57–62] Indeed, the dielectric function of $SrTiO_3$ supports high-quality SPhP across the entire wavelength range from 20 to 60 µm (5–15 THz) across the entire temperature range of 20–300 K.[63,64] The combination of broad bandwidth, low loss, and temperature insensitivity relies on quantum paraelectricity because, without quantum fluctuations, the condensation of soft phonons in materials with broad Reststrahlen bands such as $BaTiO_3$ and $KNbO_3$ leads to lossy, temperature-dependent, and anisotropic optical properties. Among known quantum paraelectric materials, $SrTiO_3$ is the best for phonon polaritonics, because its additional phonon resonance inside the Reststrahlen band of the soft mode (≈5 THz) is relatively weak, unlike $KTaO_3$ which has a strong lossy resonance at 6 THz.[65] As a proof of concept, we designed $SrTiO_3$-based ultrafast SPhP concentrators compatible with high THz fields and all polarizations. The design uses a patterned dielectric layer to modulate SPhP without micromachining the flat, single-crystalline $SrTiO_3$ substrate itself. To launch SPhP from free space, we used coupled mode theory to determine the optimal dielectric thickness and established a quasi-phase matching condition to determine the planar geometry. Numerical simulation results showed that the concentrators can coherently enhance incoming focused THz fields by another order of magnitude with a wide frequency tunability from 7 to 13 THz. In contrast to tip or gap enhancement in previous PhP resonators, the peak field of the concentrator is distributed in an area large enough for far-field optical spectroscopy. We then experimentally verify the temperature-insensitive field enhancement with THz-field-induced second harmonic generation (TEFISH) spectroscopy. Finally, we demonstrate an intense, multicycle THz field of 0.5 GV m^{-1} with the SPhP device in a tabletop setup without any sign of damage or nonlinearity. Our results may inspire new types of THz photonics to facilitate quantum materials engineering and on-chip molecular sensing.

2. Results and Discussion

The generation and propagation of SPhP requires a negative permittivity of materials, analogous to surface plasmon polariton (SPP).[25] Unlike SPP in metals or highly-doped semiconductors, SPhP is particularly suitable for sub-wavelength applications in far-infrared frequencies, where dielectrics have a much better permittivity match with the environments.[25,30] SPhP also exhibits a smaller damping rate due to a longer phonon scattering lifetime.[25,29] Last, SPhP dielectrics can potentially sustain extremely intense electric fields (≈GV m^{-1}), when plasmonic resonators may break down due to field emission from metals.[24] However, the drawback of conventional PhP materials is their relatively narrow bandwidth compared with plasmonics. **Figure 1** summarizes the PhP properties of typical dielectrics and corresponding inverse dielectric loss tangent $\tan^{-1}\delta = Re(\epsilon_r)/Im(\epsilon_r)$, which is sometimes called the quality factor of the materials, calculated based on data from previous literature.[26,34,41,45,47,66–71] The useful PhP band of the materials is chosen to be the wavelength range where the loss tangent is less than 4 times the minimal value. Among all polaritonic materials in the same spectral range, single-crystalline $SrTiO_3$ exhibits the broadest coverage with the highest quality. This makes $SrTiO_3$ an excellent material platform for phonon polaritonics in the new THz gap.

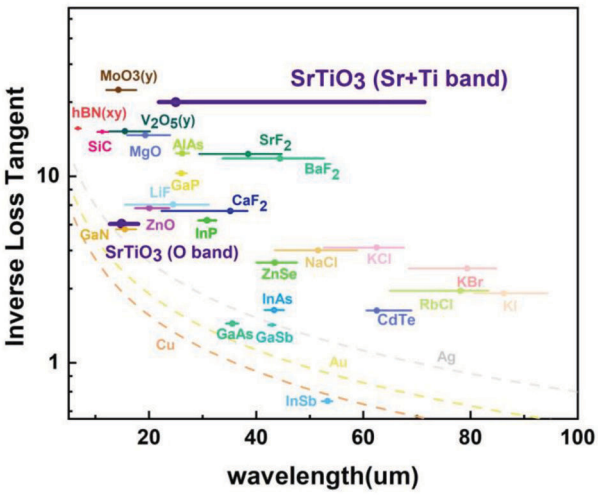

Figure 1. The Reststrahlen band of typical dielectrics and corresponding quality (inverse dielectric loss tangent) of surface phonon polaritons in infrared and terahertz region. The dots mark the minimal loss tan δ_m at the corresponding wavelength λ_m for each material. The horizontal lines indicate the wavelength range in which $\tan\delta(\lambda)$ remains smaller than $4\tan\delta_m$. $SrTiO_3$ exhibits the broadest Reststrahlen band and the lowest dielectric loss in isotropic materials, providing more freedom for phonon polaritonic engineering. For comparison, the loss of plasmon polaritons in some metals is also shown in dashed lines, which are significantly higher than phonon polaritons.

A technical challenge for the development of $SrTiO_3$ photonic devices is the difficulty to deposit or pattern high-quality single crystals. For traditional phonon–polariton structures, the etching and patterning of the substrate material itself are necessary,[26,72,73] but the process would create surface defects and may increase loss. Fortunately, it is possible to control SPhP by dielectric layers on top of flat bulk substrates like the scheme previously shown in the mid-infrared region.[34] In this work at THz frequency, we simply choose the SU-8 photoresist as the dielectric coating, because it enables direct patterning of gratings with variable thickness via standard photolithography, and exhibits a relatively low dielectric loss in THz frequencies.[74] **Figure 2**a illustrates our SPhP concentrator designed to magnify a focused, THz pulse with a Gaussian beam profile at normal incidence

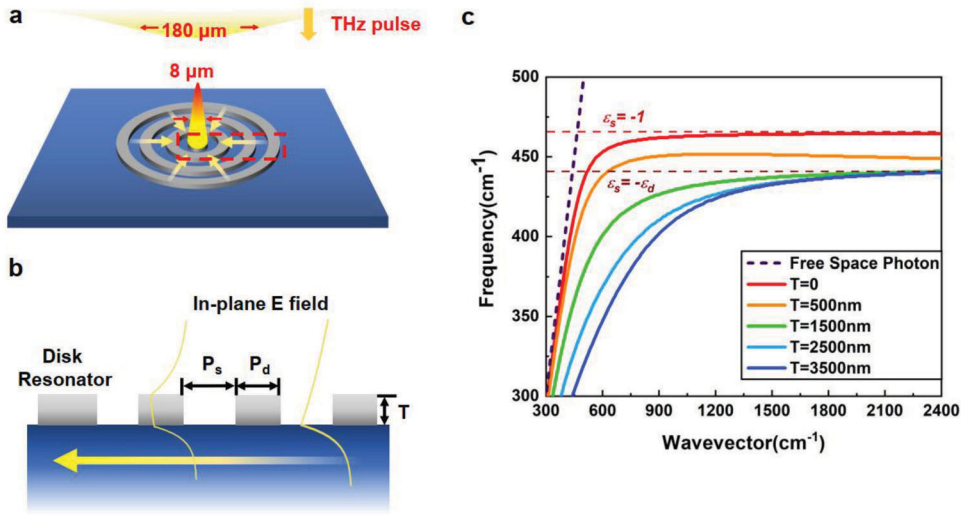

Figure 2. a) The schematic diagram of the polarization-independent SPhP concentrators made of $SrTiO_3$. Dielectric concentric ring gratings are deposited on top of the single-crystalline PhP substrate to launch and focus SPhP propagating toward the central disk resonator. The sizes are taken from the device working at 11 THz. b) Cross-sectional view of the concentrator in the red dashed box in (a). The vertical distributions of the in-plane electric field (E_x, yellow solid line) exhibit large contrast between the SU-8 ridge and the air groove regions, allowing incident plane waves to couple into the grating. The resonant frequency of the grating can be tuned by the geometrical parameters, including the widths of the ridges (P_d) and grooves (P_s), as well as the thickness (T) of the ridges. c) The SPhP dispersion in air/$SrTiO_3$ interface and air/SU-8/$SrTiO_3$ structure with varying SU-8 thickness T. The large wavevector of the SPhP in multilayer allows subwavelength compression of the incoming terahertz pulses.

from the free space. A series of concentric ring gratings couple the incident electric field in phase to SPhP (Section 4, Supporting Information) and guide the energy to a central disk resonator. The resonance frequency of the coupler and the resonator can be tuned by varying their widths and thickness, as shown in the vertical cross-section in Figure 2b. The SU-8 layer itself has a moderate dielectric constant of 3.28 near 10 THz and a thickness much smaller than the wavelength of incident light. Without the SPhP substrate, SU-8 gratings have tiny scattering power and do not support subwavelength confinement (Section 7, Supporting Information). Therefore, we emphasize that the key coupling mechanism is the modification of the SPhP field profile by the SU-8 (yellow solid lines in Figure 2b). The penetration depth of the SPhP field is less than 2 μm into the $SrTiO_3$ substrate, which can be regarded as semi-infinite. The rotational symmetric geometry allows the concentrator to coherently magnify round beams with arbitrary polarizations and preserve the polarization of the electric field inside the central resonator, as opposed to previously reported THz rectangular slit[75,76] or split ring resonator,[24,77] which only work for one linear polarization. Similar bull's eye antennae have been investigated to enable efficient collection of SPP energy in optical frequencies, but never experimentally demonstrated in mid- to far-infrared.[78–81] Besides the new frequency range, our work offers two other distinctions. First, the concentrators are optimized to match the spatial and spectral profile of multicycle THz pulses to achieve not only spectral enhancement but also an intense transient field, which is crucial for non-equilibrium processes such as Floquet engineering.[82] A spatial match means that the size of the concentrator is larger than the beam size of the THz pulse to ensure efficient coupling. Spectral match means that the bandwidth of the concentrator is comparable to that of the incident pulse. Bandwidth matching is important because there is a trade-off between transient field magnitude and spectral intensity for high-quality resonators. The spectral intensity scales with the quality factor Q, but the ring-down time also scales with Q, such that the field strength scales with $Q^{-1/2}$. On the contrary, if resonator Q is much lower than the incident pulse, then both the spectral intensity and field amplitude reduce with lower Q. Therefore, the transient field strength is optimized at matching bandwidth. Second, the area with nearly uniform field enhancement exceeds a few μm^2, which is far-field resolvable by optical probes and facilitates advanced spectroscopy without the need for near-field setups and/or complicated interpretations.[38,76,83]

We first optimized the SPhP grating couplers according to quasi-phase matching and coupled mode theory. The quasi-phase matching is determined by the width of the dielectric ridges (P_d) and grooves with the bare substrate (P_s) analogous to previous SPP works.[81,84] However, unlike SPP in this wavelength range, the wavevectors of SPhP in the ridge (k_d) and groove regions (k_s) are very different and must be treated separately (Figure 2c). For an incoming beam at normal incidence, the maximum coupling occurs when the SPhP experiences opposite phases in the ridges and grooves, that is, $k_d \times P_d = k_s \times P_s = \pi$. For any desired resonance frequency ω_0, the SPhP dispersion $k_s(\omega) = k_0\sqrt{\frac{\epsilon_s(\omega)}{\epsilon_s(\omega)+1}}$ at the bare interface of PhP substrate and $k_d(T)$ at the dielectric layers with various thickness T are shown in Figure 2c. Here $\epsilon_s(\omega)$ is the real part of the permittivity of the PhP substrate, and $k_d(T)$ is calculated by transfer matrix method analogous to previous works[85,86] (Section 15, Supporting Information). The optimal thickness of the grating is determined by the coupled mode theory so that the energy transfer from the free space to the concentrator is maximized at the critical coupling. The coupling between

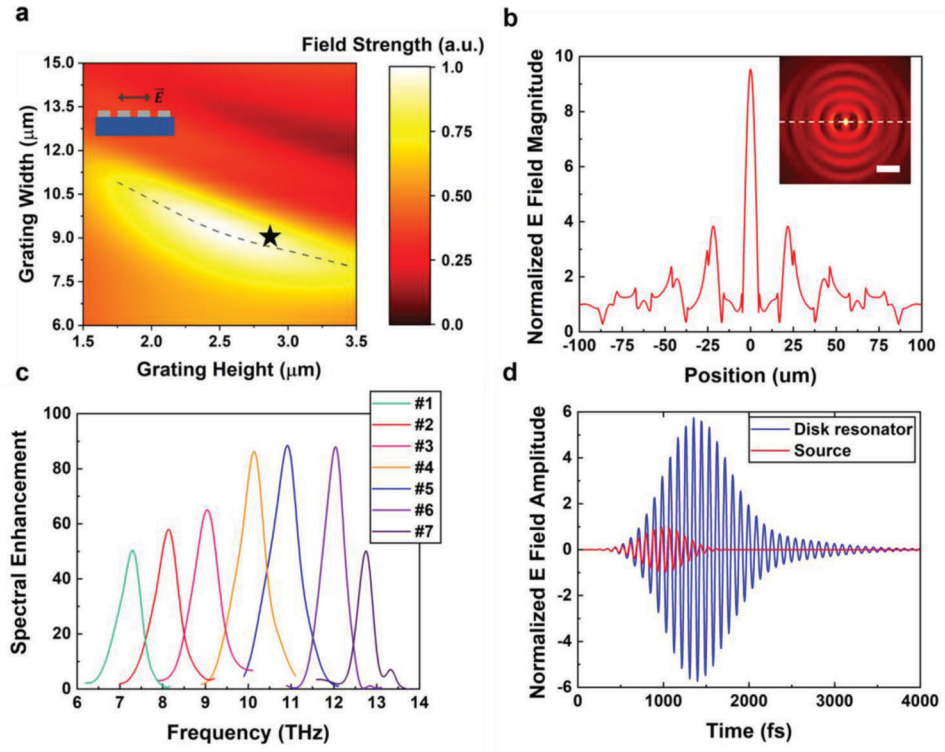

Figure 3. Designing ultrafast concentrators that maximize the transient electric field of broadband, transformation-limited terahertz pulses. a) The field strength at the center frequency of 11 THz at the center of the grating as a function of ridge width (P_d) and height (T) simulated for a 2D grating model. The dashed line indicates the quasi-phase matching condition. The optimal thickness, linked with the coupling strength of the grating, is determined from the lateral size of the light source according to the coupled mode theory. The star indicates the optimal geometry found by 3D simulation, which slightly deviates from the 2D model due to curved wavefront and non-uniform illumination. The inset indicates the polarization of the incident light, which is along the grating vector. b) Cross-sectional view and 2D top view (inset) of E-field enhancement for a horizontally polarized incident pulse at the center frequency. The field magnitude is normalized by that of the free-space THz source. Scale bar: 30 μm. c) The peak spectral enhancement of ultrafast concentrators designed across a broad range between 7 and 13 THz. d) The local enhancement of the transient E-field by up to 6 times at the center of concentrator #5 compared to a normalized incident pulse with a bandwidth of 1 THz.

the incident field and the SPhP is proportional to the dielectric contrast of the grating, which should be optimized according to the lateral size of the incident beam. We first simulated the field strength in the SPhP gratings, which increases with the coupling efficiency, at different frequencies with varying thickness and the width of the dielectric ridges P_d by 2D finite-difference time-domain method (See Experimental Section). Here $P_s = \frac{\pi}{k_s}$ is fixed to simplify the optimization. **Figure 3**a shows the field strength at the center of a SU-8 grating on top of $SrTiO_3$ for an incident Gaussian pulse with a full width at half maximum (FWHM) of 180 μm and a center frequency at 11 THz. The dashed line indicates the theoretical quasi-phase matching condition, which matches well with the numerical result. The maximum percentage of energy dissipated inside the grating, corresponding to the highest field strength, is 68% for transverse-magnetic polarization with a grating thickness ≈2.6 μm. The remaining energy is either reflected back into the air or launched into the SPhP mode at the air/$SrTiO_3$ interface from the outer edge of the grating. The optimal thickness from 2D simulation can be obtained for the frequency range of 7–13 THz (Section 1, Supporting Information), which is the starting point for designing the 3D bull's eye concentrators.

Next, to achieve large transient field enhancement, we simultaneously optimized the diameter of the central disk resonator and refined the thickness of the entire concentrator in full-scale 3D simulation. Both the disk resonator and the surrounding ring grating have matching frequency and bandwidth with the experimentally generated THz pulses so that all frequency components are coherently enhanced. The star in Figure 3a marks the final choice of geometry (T = 2.8 μm and P_d = 9 μm). The main difference between 3D and 2D structures is that the coupling efficiency does not depend on incident polarization, but roughly half of the energy is immediately reflected from the grating area where the polarization is effectively transverse-electric. The field profiles in both the incoming beam and SPhP also significantly deviate from the ideal 2D coupled mode theory. Nevertheless, about one-fourth of the energy at the center frequency coupled into the concentrator is eventually delivered to the disk resonator and dissipated by dielectric loss (Section S5, Supporting Information). The peak magnitude of the electric field, measured at the center of the top surface of the resonator, reaches ≈10 times the free space value at the center frequency (Figure 3b). The energy is also distributed over a large volume with a spatial FWHM of 8 μm, sufficient for far-field optical probes. The results are also

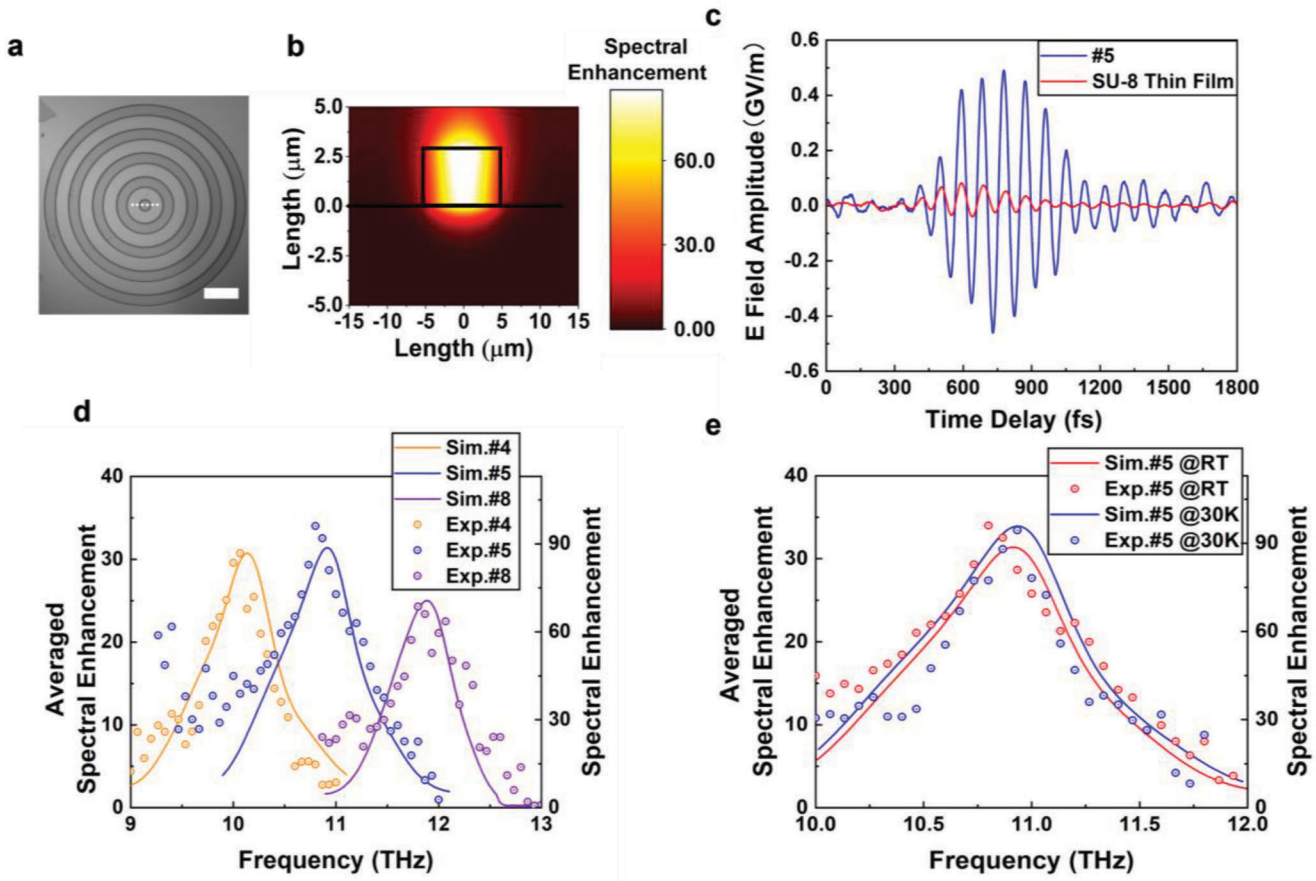

Figure 4. Experimental demonstration of coherent THz field enhancement inside the ultrafast concentrators by TEFISH. a) The optical image of the fabricated device #5. Scale bar: 30 μm. b) Cross-sectional view of the simulated spectral enhancement at the resonant frequency in the center disk marked by a white dashed line in (a). c) Time-resolved TEFISH signal averaged in the center disk compared with the TEFISH signal obtained from a SU-8 thin film of the same thickness, showing sixfold enhancement and reaching up to 0.5 GV m^{-1}. d) The averaged spectral enhancement across the central disks in three devices designed for different resonant frequencies. The experimental results agree well with the simulations, demonstrating excellent tunability of the devices. For simplicity of fabrication and measurement, device #8 has sub-optimal thickness compared with #6, resulting in less enhancement than Figure 3c (see Experimental Section). e) The spectral enhancement is nearly unchanged in cryogenic temperatures.

polarization-insensitive due to the symmetric ring structure, ensuring the magnification performance applies to the THz pulse with any polarization (Section 9, Supporting Information). We define spectral enhancement as the ratio between the spectral energy density $\epsilon_0 E^2(\omega)$ to that of the incident THz source $\epsilon_0 E_0^2(\omega)$ at the center of the beam, which reaches up to 90 at 11 THz over the top surface of the central disk (Figure 3c). The central disk alone can offer 5–7 times of enhancement, and the remaining enhancement factor comes from the grating coupler (Section 6, Supporting Information). Comparable enhancement can be realized within a broadband of 7.3 to 12.7 THz with seven different sets of T, P_d, and P_s (devices #1 to #7 with parameters in Table S1, Supporting Information). Finally, considering the enhancement of all the spectral components, we found the amplitude of the instantaneous field $E_x(t)$ in concentrator #5 is locally enhanced by a factor of 6 (Figure 3d, Section 2, Supporting Information), indicating excellent in-phase superposition from different frequency components. Transient field enhancement is more important for studying nonlinear phenomena in materials but is also more difficult to achieve than spectral enhancement, which can be simply increased by resonators with higher quality factors. We also emphasize that the disk and grating structure itself without $SrTiO_3$ substrate cannot enhance the THz field (Section S7, Supporting Information). The SU-8 dielectric layer can neither support a confined waveguide mode nor make an efficient Fresnel phase plate. The phonon–polaritonic substrate and the SPhP mode are indispensable for the deep sub-wavelength field confinement and the large enhancement.

To experimentally verify our design and quantitatively characterize the THz field enhancement of the ring cavities, we measure the amplitude of the local THz field in the fabricated SPhP concentrator (**Figure 4**a) by phase-sensitive, heterodyne THz-field induced second harmonic generation (TEFISH) (See Experimental Section).[87] Both $SrTiO_3$ and SU-8 are centrosymmetric materials, and thus do not have intrinsic second harmonic generation. The THz electric field inside the materials induces an effective second-order nonlinearity according to $\chi^{(2)} = E_{THz}\,\chi^{(3)}$, which is probed by a far-field pulse with the center wavelength of 800 nm. The spot size of the probe pulse covers the entire central disk but is still sub-wavelength with respect to the THz

field. At this probe wavelength, the $\chi^{(3)}$ nonlinearity of SU-8 is much stronger than that of $SrTiO_3$. Therefore, the generated second harmonic signal represents the average E_{THz} value inside the SU-8 disk resonator. Numerical simulation shows that the average spectral enhancement is approximately one-third of the peak spectral enhancement at the top surface of the disk resonator (Figure 4b, Experimental Section). Figure 4c shows the averaged time-resolved TEFISH signal in the central disk of device #5 and that in a SU-8 thin film on fused silica as the reference. The free-space multicycle pump pulse is centered at 11 THz with an FWHM of 1 THz and has a peak electric field of 0.1 GV m^{-1} (See Experimental Section). Thus, the field inside the SU-8 film is 82% of the incident field, or 0.08 GV m^{-1}, due to reflectance according to numerical simulation (Section 8, Supporting Information). We observe that the instantaneous field amplitude in device #5 is enhanced by sixfolds compared with that in the SU-8 thin film. Therefore, the average in-plane electric field reaches 0.5 GV m^{-1} inside the disk resonator and the net enhancement from the free-space field is ≈5 times. The main envelope of the incoming multicycle pulse is largely preserved in the concentrator, showing good temporal coherence during SPhP propagation and negligible THz polarization dependence (Section 9, Supporting Information).

To analyze the spectral enhancement of the concentrators, we apply Fast Fourier Transform to the time-domain signal from both the SPhP concentrators and the thin film (Section 10, Supporting Information). We then take the ratio of the spectral intensity and convert the ratio to the averaged spectral enhancement with respect to the free-space pulses. The average enhancement of 32 corresponds to the peak enhancement of 90 on the top surface, which also agrees with the simulation (Figure 4d). Moreover, we experimentally verified that the spectral enhancement for concentrators designed in other frequencies (Section 11, Supporting Information) all agree well with the simulation in terms of enhancement ratio and linewidth. A minor redshift of resonance frequency may be due to either a small thickness deviation of the SU-8 coating or the error in dielectric functions of SU-8 and $SrTiO_3$ used in simulations, which are based on previous literature, from their actual value in experimental conditions. Precise determination of dielectric functions may be conducted via techniques such as broadband THz time-domain spectroscopy or spectroscopic ellipsometry in the future.[88] For simplicity of fabrication and measurement, all concentrators are fabricated together on one chip with the same dielectric thickness of 2.8 μm. At 10 THz, the thickness is very close to the optimal value (Section 1, Supporting Information). Meanwhile, at 12 THz, where the optimal thickness is 2 μm in device #6, the enhancement is slightly less in device #8, but remains robust and agrees with the simulation using sub-optimal thickness. These results prove that the $SrTiO_3$ SPhP concentrators can provide intense periodic THz fields easily accessible by far-field optical spectroscopy, as well as wide tunability within the new terahertz gap.

We observed no sign of damage to either the dielectric layer or the substrate under the intense field, demonstrating the advantage of phonon polaritonic devices over plasmonic structures to study nonlinear physics. We note that the maximum ionic displacement in $SrTiO_3$ in our experimental condition is $\frac{e^* E}{\omega^2 M} \approx 4$ pm, where $e^* = 1.18 \times 10^{-18}$ C and $M = 3.11 \times 10^{-26}$ kg are the effective charge and mass of the soft phonon mode, respectively.[89] This displacement is not insignificant compared with the typical ferroelectric displacement of ≈10 pm and may induce an anharmonic shift to the soft phonon mode itself. Fortunately, the non-resonant dielectric function above 7 THz is insensitive to such shifts (Section 13, Supporting Information). Therefore, we do not expect the performance of SPhP concentrators to show nonlinearity in our experimental conditions, which is also experimentally confirmed (Section 12, Supporting Information). Last, we also confirmed that phonon polaritonics based on $SrTiO_3$ works for a wide temperature range, despite the material having complex phase transitions in cryogenic temperatures, and the dielectric function being known to be temperature-dependent due to phonon-softening.[7,64,90] As the changes in dielectric function are minor above 7 THz[64] (Section 13, Supporting Information), the concentrator's performance should exhibit negligible temperature dependence. Figure 4e shows the comparison of THz field response spectra of device #5 at room temperature and at 30 K, where the phonon softening saturates in the quantum paraelectric phase.[91] Indeed, both simulated and experimentally measured spectra show almost identical center frequency, enhancement factor, and FWHM as designed at the two temperatures. The stable performance of SPhP concentrators can support future studies of non-equilibrium quantum materials in these extreme conditions.

The performance of the SPhP concentrators, such as the transient field enhancement, uniformity of the field, and spectral enhancement may be further adjusted or improved according to the design principles illustrated in this work by introducing new materials and structures. For example, dielectric materials with very low loss in the target frequencies, including hydrocarbon polymers ($\tan\delta = 0.003$)[88] and tellurium ($\tan\delta = 1.6 \times 10^{-4}$),[92] are promising to replace SU-8 ($\tan\delta = 0.06$) for the modulation of SPhP. By reducing the dielectric loss, the spectral enhancement can be boosted by another factor of 3 (Section 14, Supporting Information). When the coupler's loss is reduced, additional Bragg reflectors outside the concentrators will provide significant contributions to the energy collection. Finally, to achieve polarization-independent, extremely intense electric fields, the central disks may be replaced by resonators with higher confinement factors, like dual-arm bowtie antennas working in the large-wavevector regime in the SPhP dispersion curve.[81,93,94]

3. Conclusion

In summary, we experimentally proved the concept of phonon–polaritonics in the "new terahertz gap" frequencies based on single-crystalline quantum paraelectric $SrTiO_3$. We realized polarization-independent THz field concentrators using simple design principles of quasi-phase matching condition and coupled mode theory, along with a fabrication process that minimized materials damage. The concentrator resonantly enhances multi-cycle THz pulses to achieve an intense periodic electric field on the order of GV m^{-1} over a volume that is optically resolvable without the need for near-field microscopy. The methodology is not limited to $SrTiO_3$ but can be generalized to cover electronic, vibrational, or spin resonances over 3.3–19 THz using other commercially available, polished single-crystalline SPhP substrates listed in Figure 1, or materials with reduced fabrica-

tion challenges, which may still function for narrowband applications with acceptable performance. Finally, we envision that such SPhP devices can be easily integrated with a wide range of specimens, which can be directly placed on the disk resonators and coupled to the strong THz fields, for condensed matter physics and biomaterials research in the future.

4. Experimental Section

Numerical Simulation: Numerical simulations were conducted via commercial Finite-Difference Time-Domain software (Lumerical). The dielectric functions of $SrTiO_3$ and SU-8 in the THz region were acquired from previous literature.[64,74] Gaussian beam source with parameters close to the experiments was used. PML boundary condition, which absorbed all the electromagnetic energy reaching the boundary of the simulation region with minimal reflection, was applied to all the boundaries to study the performance of single-ring concentrators. The lateral dimension of the simulation region was 400 μm × 400 μm, which was twice the size as the concentrator structure and was large enough to avoid artifacts from the PML boundaries. Convergence tests regarding simulation regions, mesh size, and simulation time were carefully checked for the accuracy of results. Both time and electric field monitors were placed at the top surface of the central disk for data collection. Averaged spectral enhancement was acquired by calculating the square of averaged E field enhancement at each frequency within the central disk volume. Since the field distribution was almost the same along the *z*-direction (Figure 4b), the integration could be simplified as extracting data at the top surface.

SPhP Concentrator Fabrication: Nanofabrication of the THz SPhP concentrator was conducted in the Nano-Fab Clean Room at Rice Shared Equipment Authority. As-grown, single-crystalline, double-side polished $SrTiO_3$ in ⟨100⟩ orientation with a size of 10 mm × 10 mm and a total thickness of 0.5 mm was purchased from Biotain Crystal. SU-8 6002 (Kayaku Advanced Materials) was used as purchased and spin coated on SrTiO3. The solution was first spread out to uniformly cover the $SrTiO_3$ substrate with a spin speed of 500 rpm for 5 s, and then increased to 3200 rpm for 60 s, giving a final desired thickness of ≈2.8 μm, as designed for Concentrator #5. Prior to the photolithography, SU-8 was soft-baked under 110 °C for 3 min. The ring patterns were written by maskless photo-lithography (Bruker SF-100 Lightning) under 365 nm ultraviolet light emitting diode exposure with built-in intensity in the system and an exposure time of 0.76 s. The geometrical parameters of the patterns can be found in Section 3 (Supporting Information). Patterned devices were then post-baked under 110 °C for 2 min and developed in SU-8 developer (Kayaku Advanced Materials, used as purchased) for 3 min. The sample was then rinsed with a fresh developer for another 30 s and dried with pressurized nitrogen. Dose tests were also conducted for optimal exposure quality and reproductivity.

TEFISH Measurements: Details for the TEFISH setup (Section 16, Supporting Information) are described elsewhere.[87] Briefly, the frequency-adjustable, intense, narrowband multicycle THz pulse in the new THz gap was generated by chirped-pulse difference frequency generation in DAST. The THz beam was focused onto the sample with a spot size of 180 μm by a set of three parabolic mirrors. The fluency of the pulse was measured to be 600 μJ cm^{-2} with a pulse width of 350 fs. This gave a peak E field of ≈0.1 GV m^{-1}. The probe pulses with a center wavelength of 800 nm and a duration of 40 fs were co-focused on the sample with a spot size of 30 μm. For the heterodyne TEFISH detection of THz electric field, a local oscillator (LO) field of 400 nm was produced by a 10 μm-thick Barium Borate (BBO) crystal and co-propagate with the probe beam. The interference of the TEFISH field $E_{2\omega}^{\mathrm{TEFISH}} = \chi_{\mathrm{sample}}^{(3)} E_{\omega}^{2} E_{\mathrm{THz}}$ with the LO field $E_{2\omega}^{\mathrm{LO}}$ results in a total signal intensity $I_{2\omega}^{\mathrm{Total}}$, which was given by:

$$I_{2\omega}^{\mathrm{Total}} \propto (E_{2\omega}^{\mathrm{TEFISH}} + E_{2\omega}^{\mathrm{LO}})^2$$

$$\propto \left[\left(\chi_{\mathrm{sample}}^{(3)} I_{\omega} \right)^2 I_{THz} + 2\chi_{\mathrm{sample}}^{(3)} I_{\omega} E_{THz} E_{2\omega}^{LO} + (E_{2\omega}^{LO})^2 \right] \quad (1)$$

where $\chi_{\mathrm{sample}}^{(3)}$ is the third nonlinear optical susceptibility of the measured sample (SU-8 in our case), E_{THz} (E_{ω}) is the electric field magnitude of the THz source (800 nm probe), and I_{THz} (I_{ω}) denotes the intensity of the THz source (800 nm probe).

When the LO was set to be much stronger than TEFISH, the change in signal was dominated by the interference term. Therefore, the measured oscillating signal was approximately proportional to the THz field inside the sample volume:

$$\Delta I_{2\omega} \propto \chi_{\mathrm{sample}}^{(3)} I_{\omega} E_{THz} E_{2\omega}^{LO} \quad (2)$$

Here it was assumed that the probe pulses were much shorter than the periodicity of the THz field. As a result, both the amplitude and phase information could be obtained by this heterodyne detection. The output signal $\Delta I_{2\omega}$ was filtered by a series of 400 nm bandpass filters and detected by a photomultiplier tube. The TEFISH signal mainly came from SU-8 and its intensity was linearly proportional to the average THz field inside the probe spot. A flat SU-8 thin film was used on fused silica with the same thickness as the concentrators as the reference sample, whose electric field was 82% of the free-space THz pulse (Section 8, Supporting Information). The signal was also normalized by the area of SU-8 covered by the probe.

Supporting Information

Supporting Information is available from the Wiley Online Library or from the author.

Acknowledgements

R.X., X.C., and H.Z. are supported by the U.S. National Science Foundation (NSF) under award number DMR-2005096. T.L., J.L., and H.Z. are supported by the Welch Foundation under grant number C-2128. E.B. is supported by the Graduate Research Fellowship Program (GRFP) from U.S. National Science Foundation (NSF) under grant number DGE-1842494. A.M. is supported by the Nano REU program from the U.S. National Science Foundation (NSF) under grant number EEC-1757967. The authors thank Dr. Yiming Yang's research group from Dalian University of Technology, China for helpful discussion and Mr. Andrea Donohue from J.A. Woollam Co., Inc for assistance in measuring the dielectric function of the $SrTiO_3$ crystals used in this work.

Conflict of Interest

The authors declare no conflict of interest.

Author Contributions

R.X. and H.Z. conceived the project and experiment. R.X. carried out numerical simulations. R.X., J.L., A.M., and K.J. fabricated the samples. T.L. and X.C. performed TEFISH experiments. R.X. and H.Z. analyzed the simulation and experimental data. R.X., T.L., E.B., and H.Z. wrote the manuscript with input from all authors.

Data Availability Statement

The data that support the findings of this study are available in the supplementary material of this article.

Keywords

driven quantum materials, nonlinear spectroscopy, phonon polaritons, strontium titanate, terahertz photonics

Received: March 31, 2023
Revised: June 8, 2023
Published online: July 2, 2023

[1] S. S. Dhillon, M. S. Vitiello, E. H. Linfield, A. G. Davies, M. C. Hoffmann, J. Booske, C. Paoloni, M. Gensch, P. Weightman, G. P. Williams, E. Castro-Camus, D. R. S. Cumming, F. Simoens, I. Escorcia-Carranza, J. Grant, S. Lucyszyn, M. Kuwata-Gonokami, K. Konishi, M. Koch, C. A. Schmuttenmaer, T. L. Cocker, R. Huber, A. G. Markelz, Z. D. Taylor, V. P. Wallace, J. A. Zeitler, J. Sibik, T. M. Korter, B. Ellison, S. Rea, et al., *J. Phys. D: Appl. Phys.* **2017**, *50*, 043001.
[2] A. Leitenstorfer, A. S. Moskalenko, T. Kampfrath, J. Kono, E. Castro-Camus, K. Peng, N. Qureshi, D. Turchinovich, K. Tanaka, A. Markelz, M. Havenith, C. Hough, H. J. Joyce, W. Padilla, B. Zhou, K.-Y. Kim, X.-C. Zhang, P. U. Jepsen, S. Dhillon, M. S. Vitiello, E. H. Linfield, A. G. Davies, M. Hoffmann, R. Lewis, M. Tonouchi, P. Klarskov, T. Seifert, Y. Gerasimenko, D. D. Mihailovic, R. Huber, et al., *J. Phys. D: Appl. Phys.* **2023**, *56*, 223001.
[3] D. Hsieh, D. N. Basov, R. D. Averitt, *Nat. Mater.* **2017**, *16*, 1077.
[4] D. Nicoletti, A. Cavalleri, *Adv. Opt. Photonics* **2016**, *8*, 401.
[5] A. S. Disa, T. F. Nova, A. Cavalleri, *Nat. Phys.* **2021**, *17*, 1087.
[6] M. Budden, T. Gebert, M. Buzzi, G. Jotzu, E. Wang, T. Matsuyama, G. Meier, Y. Laplace, D. Pontiroli, M. Riccò, F. Schlawin, D. Jaksch, A. Cavalleri, *Nat. Phys.* **2021**, *17*, 611.
[7] X. Li, T. Qiu, J. Zhang, E. Baldini, J. Lu, A. M. Rappe, K. A. Nelson, *Science* **2019**, *364*, 1079.
[8] E. J. Sie, C. M. Nyby, C. D. Pemmaraju, S. J. Park, X. Shen, J. Yang, M. C. Hoffmann, B. K. Ofori-Okai, R. Li, A. H. Reid, S. Weathersby, E. Mannebach, N. Finney, D. Rhodes, D. Chenet, A. Antony, L. Balicas, J. Hone, T. P. Devereaux, T. F. Heinz, X. Wang, A. M. Lindenberg, *Nature* **2019**, *565*, 61.
[9] D. Afanasiev, J. R. Hortensius, B. A. Ivanov, A. Sasani, E. Bousquet, Y. M. Blanter, R. V. Mikhaylovskiy, A. V. Kimel, A. D. Caviglia, *Nat. Mater.* **2021**, *20*, 607.
[10] G. Acbas, K. A. Niessen, E. H. Snell, A. G. Markelz, *Nat. Commun.* **2014**, *5*, 3076.
[11] W. J. Choi, G. Cheng, Z. Huang, S. Zhang, T. B. Norris, N. A. Kotov, *Nat. Mater.* **2019**, *18*, 820.
[12] W. J. Choi, S. H. Lee, B. C. Park, N. A. Kotov, *J. Am. Chem. Soc.* **2022**, *144*, 22789.
[13] W. J. Choi, K. Yano, M. Cha, F. M. Colombari, J.-Y. Kim, Y. Wang, S. H. Lee, K. Sun, J. M. Kruger, A. F. de Moura, N. A. Kotov, *Nat. Photonics* **2022**, *16*, 366.
[14] D. A. Turton, H. M. Senn, T. Harwood, A. J. Lapthorn, E. M. Ellis, K. Wynne, *Nat. Commun.* **2014**, *5*, 3999.
[15] K. J. Tielrooij, D. Paparo, L. Piatkowski, H. J. Bakker, M. Bonn, *Biophys. J.* **2009**, *97*, 2484.
[16] E. Rowe, B. Yuan, M. Buzzi, G. Jotzu, Y. Zhu, M. Fechner, M. Först, B. Liu, D. Pontiroli, M. Riccò, A. Cavalleri, arxiv:2301.08633, **2023**.
[17] J. Luo, T. Lin, J. Zhang, X. Chen, E. R. Blackert, R. Xu, B. I. Yakobson, H. Zhu, arxiv:2306.03852, **2023**.
[18] M. Yu, S. Yan, Y. Sun, W. Sheng, F. Tang, X. Peng, Y. Hu, *Sensors* **2019**, *19*, 1148.
[19] M. Seo, J.-H. Mun, J. Heo, D. E. Kim, *Sci. Rep.* **2022**, *12*, 16273.
[20] J. Dai, X. Xie, X.-C. Zhang, *Phys. Rev. Lett.* **2006**, *97*, 103903.
[21] T. Seifert, S. Jaiswal, U. Martens, J. Hannegan, L. Braun, P. Maldonado, F. Freimuth, A. Kronenberg, J. Henrizi, I. Radu, E. Beaurepaire, Y. Mokrousov, P. M. Oppeneer, M. Jourdan, G. Jakob, D. Turchinovich, L. M. Hayden, M. Wolf, M. Münzenberg, M. Kläui, T. Kampfrath, *Nat. Photonics* **2016**, *10*, 483.
[22] M. A. Seo, H. R. Park, S. M. Koo, D. J. Park, J. H. Kang, O. K. Suwal, S. S. Choi, P. C. M. Planken, G. S. Park, N. K. Park, Q. H. Park, D. S. Kim, *Nat. Photonics* **2009**, *3*, 152.
[23] K. Iwaszczuk, A. Andryieuski, A. Lavrinenko, X.-C. Zhang, P. U. Jepsen, *Opt. Express* **2012**, *20*, 8344.
[24] M. Liu, H. Y. Hwang, H. Tao, A. C. Strikwerda, K. Fan, G. R. Keiser, A. J. Sternbach, K. G. West, S. Kittiwatanakul, J. Lu, S. A. Wolf, F. G. Omenetto, X. Zhang, K. A. Nelson, R. D. Averitt, *Nature* **2012**, *487*, 345.
[25] J. D. Caldwell, L. Lindsay, V. Giannini, I. Vurgaftman, T. L. Reinecke, S. A. Maier, O. J. Glembocki, *Nanophotonics* **2015**, *4*, 44.
[26] J. D. Caldwell, A. V. Kretinin, Y. Chen, V. Giannini, M. M. Fogler, Y. Francescato, C. T. Ellis, J. G. Tischler, C. R. Woods, A. J. Giles, M. Hong, K. Watanabe, T. Taniguchi, S. A. Maier, K. S. Novoselov, *Nat. Commun.* **2014**, *5*, 5221.
[27] J. D. Caldwell, O. J. Glembocki, Y. Francescato, N. Sharac, V. Giannini, F. J. Bezares, J. P. Long, J. C. Owrutsky, I. Vurgaftman, J. G. Tischler, V. D. Wheeler, N. D. Bassim, L. M. Shirey, R. Kasica, S. A. Maier, *Nano Lett.* **2013**, *13*, 3690.
[28] S. Foteinopoulou, G. C. R. Devarapu, G. S. Subramania, S. Krishna, D. Wasserman, *Nanophotonics* **2019**, *8*, 2129.
[29] J. B. Khurgin, *Nat. Nanotechnol.* **2015**, *10*, 2.
[30] Y. Zhong, S. D. Malagari, T. Hamilton, D. M. Wasserman, *J. Nanophotonics* **2015**, *9*, 093791.
[31] T. Taubner, D. Korobkin, Y. Urzhumov, G. Shvets, R. Hillenbrand, *Science* **2006**, *313*, 1595.
[32] H. C. Kim, X. Cheng, *Opt. Lett.* **2010**, *35*, 3748.
[33] B. Neuner, D. Korobkin, C. Fietz, D. Carole, G. Ferro, G. Shvets, *J. Phys. Chem. C* **2010**, *114*, 7489.
[34] P. Li, X. Yang, T. W. W. Maß, J. Hanss, M. Lewin, A.-K. U. Michel, M. Wuttig, T. Taubner, *Nat. Mater.* **2016**, *15*, 870.
[35] J.-J. Greffet, R. Carminati, K. Joulain, J.-P. Mulet, S. Mainguy, Y. Chen, *Nature* **2002**, *416*, 61.
[36] D. M. Juraschek, P. Narang, *Nano Lett.* **2021**, *21*, 5098.
[37] A. J. Huber, B. Deutsch, L. Novotny, R. Hillenbrand, *Appl. Phys. Lett.* **2008**, *92*, 203104.
[38] A. Huber, N. Ocelic, D. Kazantsev, R. Hillenbrand, *Appl. Phys. Lett.* **2005**, *87*, 081103.
[39] R. Hillenbrand, T. Taubner, F. Keilmann, *Nature* **2002**, *418*, 159.
[40] H. Hu, N. Chen, H. Teng, R. Yu, Y. Qu, J. Sun, M. Xue, D. Hu, B. Wu, C. Li, J. Chen, M. Liu, Z. Sun, Y. Liu, P. Li, S. Fan, F. J. García de Abajo, Q. Dai, *Nat. Nanotechnol.* **2022**, *17*, 940.
[41] A. D. Dunkelberger, C. T. Ellis, D. C. Ratchford, A. J. Giles, M. Kim, C. S. Kim, B. T. Spann, I. Vurgaftman, J. G. Tischler, J. P. Long, O. J. Glembocki, J. C. Owrutsky, J. D. Caldwell, *Nat. Photonics* **2018**, *12*, 50.
[42] S. C. Kehr, Y. M. Liu, L. W. Martin, P. Yu, M. Gajek, S.-Y. Yang, C.-H. Yang, M. T. Wenzel, R. Jacob, H.-G. von Ribbeck, M. Helm, X. Zhang, L. M. Eng, R. Ramesh, *Nat. Commun.* **2011**, *2*, 249.
[43] A. M. Dubrovkin, B. Qiang, T. Salim, D. Nam, N. I. Zheludev, Q. J. Wang, *Nat. Commun.* **2020**, *11*, 1863.
[44] S. Dai, Z. Fei, Q. Ma, A. S. Rodin, M. Wagner, A. S. McLeod, M. K. Liu, W. Gannett, W. Regan, K. Watanabe, T. Taniguchi, M. Thiemens, G. Dominguez, A. H. C. Neto, A. Zettl, F. Keilmann, P. Jarillo-Herrero, M. M. Fogler, D. N. Basov, *Science* **2014**, *343*, 1125.
[45] D. Korobkin, Y. A. Urzhumov, B. Neuner, C. Zorman, Z. Zhang, I. D. Mayergoyz, G. Shvets, *Appl. Phys. A* **2007**, *88*, 605.
[46] M. Autore, P. Li, I. Dolado, F. J. Alfaro-Mozaz, R. Esteban, A. Atxabal, F. Casanova, L. E. Hueso, P. Alonso-González, J. Aizpurua, A. Y. Nikitin, S. Vélez, R. Hillenbrand, *Light: Sci. Appl.* **2018**, *7*, 17172.
[47] K. Feng, W. Streyer, S. M. Islam, J. Verma, D. Jena, D. Wasserman, A. J. Hoffman, *Appl. Phys. Lett.* **2015**, *107*, 081108.

[48] T. G. Folland, L. Nordin, D. Wasserman, J. D. Caldwell, *J. Appl. Phys.* **2019**, *125*, 191102.
[49] A. M. Dubrovkin, B. Qiang, H. N. S. Krishnamoorthy, N. I. Zheludev, Q. J. Wang, *Nat. Commun.* **2018**, *9*, 1762.
[50] K. Ohtani, B. Meng, M. Franckié, L. Bosco, C. Ndebeka-Bandou, M. Beck, J. Faist, *Sci. Adv.* **2019**, *5*, eaau1632.
[51] K. Ohtani, M. Beck, M. J. Süess, J. Faist, A. M. Andrews, T. Zederbauer, H. Detz, W. Schrenk, G. Strasser, *ACS Photonics* **2016**, *3*, 2280.
[52] S. A. Holmstrom, T. H. Stievater, M. W. Pruessner, D. Park, W. S. Rabinovich, J. B. Khurgin, C. J. K. Richardson, S. Kanakaraju, L. C. Calhoun, R. Ghodssi, *Phys. Rev. B* **2012**, *86*, 165120.
[53] W. Streyer, K. Feng, Y. Zhong, A. J. Hoffman, D. Wasserman, *MRS Commun.* **2016**, *6*, 1.
[54] W. Streyer, S. Law, A. Rosenberg, C. Roberts, V. A. Podolskiy, A. J. Hoffman, D. Wasserman, *Appl. Phys. Lett.* **2014**, *104*, 131105.
[55] W. Zhong, R. D. King-Smith, D. Vanderbilt, *Phys. Rev. Lett.* **1994**, *72*, 3618.
[56] K. A. Müller, H. Burkard, *Phys. Rev. B* **1979**, *19*, 3593.
[57] B. Fauqué, P. Bourges, A. Subedi, K. Behnia, B. Baptiste, B. Roessli, T. Fennell, S. Raymond, P. Steffens, *Phys. Rev. B* **2022**, *106*, L140301.
[58] J.-F. Ge, Z.-L. Liu, C. Liu, C.-L. Gao, D. Qian, Q.-K. Xue, Y. Liu, J.-F. Jia, *Nat. Mater.* **2015**, *14*, 285.
[59] T. Nova, A. Disa, M. Fechner, A. Cavalleri, *Science* **2019**, *364*, 1075.
[60] C. W. Rischau, D. Pulmannová, G. W. Scheerer, A. Stucky, E. Giannini, D. van der Marel, *Phys. Rev. Res.* **2022**, *4*, 013019.
[61] D. van der Marel, F. Barantani, C. W. Rischau, *Phys. Rev. Res.* **2019**, *1*, 013003.
[62] N. Kalfagiannis, J. L. Stoner, J. Hillier, I. Vangelidis, E. Lidorikis, *J. Mater. Chem. C* **2019**, *7*, 7851.
[63] D. J. Lahneman, M. M. Qazilbash, *Phys. Rev. B* **2021**, *104*, 235433.
[64] P. Dore, G. De Marzi, A. Paolone, *Int. J. Infrared Millimeter Waves* **1997**, *18*, 125.
[65] R. C. Miller, W. G. Spitzer, *Phys. Rev.* **1963**, *129*, 94.
[66] W. Ma, P. Alonso-González, S. Li, A. Y. Nikitin, J. Yuan, J. Martín-Sánchez, J. Taboada-Gutiérrez, I. Amenabar, P. Li, S. Vélez, C. Tollan, Z. Dai, Y. Zhang, S. Sriram, K. Kalantar-Zadeh, S.-T. Lee, R. Hillenbrand, Q. Bao, *Nature* **2018**, *562*, 557.
[67] W. Kaiser, W. G. Spitzer, R. H. Kaiser, L. E. Howarth, *Phys. Rev.* **1962**, *127*, 1950.
[68] T. I. Willett-Gies, C. M. Nelson, L. S. Abdallah, S. Zollner, *J. Vac. Sci. Technol., A* **2015**, *33*, 061202.
[69] P. Yu, M. Cardona, *Fundamentals of Semiconductors: Physics and Materials Properties*, 4th ed., Springer, Berlin **2010**.
[70] E. D. Palik, *Handbook of Optical Constants of Solids, Five-Volume Set*, Elsevier, Amsterdam, **1997**.
[71] J. Taboada-Gutiérrez, G. Álvarez-Pérez, J. Duan, W. Ma, K. Crowley, I. Prieto, A. Bylinkin, M. Autore, H. Volkova, K. Kimura, T. Kimura, M.-H. Berger, S. Li, Q. Bao, X. P. A. Gao, I. Errea, A. Y. Nikitin, R. Hillenbrand, J. Martín-Sánchez, P. Alonso-González, *Nat. Mater.* **2020**, *19*, 964.
[72] R. Berte, C. R. Gubbin, V. D. Wheeler, A. J. Giles, V. Giannini, S. A. Maier, S. De Liberato, J. D. Caldwell, *ACS Photonics* **2018**, *5*, 2807.
[73] V. M. Breslin, D. C. Ratchford, A. J. Giles, A. D. Dunkelberger, J. C. Owrutsky, *Opt. Express* **2021**, *29*, 11760.
[74] E. Motaharifar, R. G. Pierce, R. Islam, R. Henderson, J. W. P. Hsu, M. Lee, *J. Infrared, Millimeter, Terahertz Waves* **2018**, *39*, 93.
[75] J. Shi, Y.-Q. Bie, W. Chen, S. Fang, A. Zong, J. Han, Z. Cao, Y. Zhang, T. Taniguchi, K. Watanabe, V. Bulović, E. Kaxiras, P. Jarillo-Herrero, E. Baldini, K. A. Nelson, arxiv: 1960.13609, **2022**.
[76] F. H. Feres, R. A. Mayer, L. Wehmeier, F. C. B. Maia, E. R. Viana, A. Malachias, H. A. Bechtel, J. M. Klopf, L. M. Eng, S. C. Kehr, J. C. González, R. O. Freitas, I. D. Barcelos, *Nat. Commun.* **2021**, *12*, 1995.
[77] H.-T. Chen, J. F. O'Hara, A. J. Taylor, R. D. Averitt, C. Highstrete, M. Lee, W. J. Padilla, *Opt Express* **2007**, *15*, 1084.
[78] H. J. Lezec, A. Degiron, E. Devaux, R. A. Linke, L. Martin-Moreno, F. J. Garcia-Vidal, T. W. Ebbesen, *Science* **2002**, *297*, 820.
[79] E. Laux, C. Genet, T. Skauli, T. W. Ebbesen, *Nat. Photonics* **2008**, *2*, 161.
[80] J. Qi, T. Kaiser, A. E. Klein, M. Steinert, T. Pertsch, F. Lederer, C. Rockstuhl, *Opt. Express* **2015**, *23*, 14583.
[81] N. Rahbany, W. Geng, R. Bachelot, C. Couteau, *Nanotechnology* **2017**, *28*, 185201.
[82] T. Oka, S. Kitamura, *Annu. Rev. Condens. Matter Phys.* **2019**, *10*, 387.
[83] A. Mancini, C. R. Gubbin, R. Berté, F. Martini, A. Politi, E. Cortés, Y. Li, S. De Liberato, S. A. Maier, *ACS Nano* **2020**, *14*, 8508.
[84] S. Joseph, S. Sarkar, J. Joseph, *ACS Appl. Mater. Interfaces* **2020**, *12*, 46519.
[85] Q. Zhang, Z. Zhen, Y. Yang, G. Gan, D. Jariwala, X. Cui, *Opt. Express* **2019**, *27*, 18585.
[86] M. A. Huber, F. Mooshammer, M. Plankl, L. Viti, F. Sandner, L. Z. Kastner, T. Frank, J. Fabian, M. S. Vitiello, T. L. Cocker, R. Huber, *Nat. Nanotechnol.* **2017**, *12*, 207.
[87] T. Lin, R. Xu, X. Chen, Y. Guan, M. Yao, X. Li, H. Zhu, Optica Open. Preprint. 22066295, **2023**.
[88] P. D. Cunningham, N. N. Valdes, F. A. Vallejo, L. M. Hayden, B. Polishak, X.-H. Zhou, J. Luo, A. K.-Y. Jen, J. C. Williams, R. J. Twieg, *J. Appl. Phys.* **2011**, *109*, 043505.
[89] I. Katayama, H. Aoki, J. Takeda, H. Shimosato, M. Ashida, R. Kinjo, I. Kawayama, M. Tonouchi, M. Nagai, K. Tanaka, *Phys. Rev. Lett.* **2012**, *108*, 097401.
[90] A. A. Sirenko, C. Bernhard, A. Golnik, A. M. Clark, J. Hao, W. Si, X. X. Xi, *Nature* **2000**, *404*, 373.
[91] D. A. Tenne, A. Soukiassian, X. X. Xi, H. Choosuwan, R. Guo, A. S. Bhalla, *Phys. Rev. B* **2004**, *70*, 174302.
[92] R. S. Caldwell, H. Y. Fan, *Phys. Rev.* **1959**, *114*, 664.
[93] H. Chen, A. M. Bhuiya, R. Liu, D. M. Wasserman, K. C. Toussaint, *J. Phys. Chem. C* **2014**, *118*, 20553.
[94] M. R. Hasan, O. G. Hellesø, *Nanotechnology* **2021**, *32*, 202001.

